PHYSICAL REVIEW B VOLUME 44, NUMBER 7 15 AUGUST 1991-I

Electronic wave functions and electron–confined-phonon matrix elements in GaAs/Al_xGa_{1-x}As double-barrier resonant-tunneling structures

P. J. Turley and S. W. Teitsworth
Department of Physics, Duke University, Durham, North Carolina 27706
(Received 6 August 1990; revised manuscript received 26 November 1990)

We have numerically studied spatial properties of electronic wave functions in GaAs/Al_xGa_{1-x}As double-barrier resonant-tunneling (DBRT) structures, particularly those properties which strongly affect the interaction of electrons with confined phonon modes in the barrier and quantum-well layers and play a role in phonon-assisted tunneling. We use a transfer-matrix approach to examine the detailed spatial structure of DBRT electronic wave functions for various injection energies and applied voltages in two representative structures. In addition to verifying expected behavior for transmission probability and scattering phase shift versus energy, we find that, off resonance, the electronic wave functions show significant spatial asymmetry in the well layer, which enhances coupling of electrons to shorter-wavelength confined phonon modes. A formula for the excess current due to phonon-assisted tunneling is given. Finally, we present numerical evaluations of the matrix elements which describe the electron–confined-LO-phonon interaction for lower-order confined modes and these indicate that phonon emission occurs preferentially in the GaAs well and not the Al_xGa_{1-x}As barrier layers for typical DBRT structures.

I. INTRODUCTION

Over the past few years there has been considerable interest in predicting the current-voltage characteristics of double-barrier resonant-tunneling (DBRT) structures. Many techniques have been applied to the problem including the Wigner function,[1] the density matrix,[2] the transfer Hamiltonian approach,[3] and the Tsu-Esaki scattering approach.[4] Although these techniques have provided general qualitative agreement with experimental results, quantitative agreement is still lacking. The discrepancies are due to a range of causes including space-charge effects, elastic scattering of electrons by interfaces and impurities, and the inelastic scattering of electrons by longitudinal-optical (LO) phonons.[5–9]

One of the more striking effects associated with the electron–LO-phonon interaction is a phenomenon known as phonon-assisted tunneling. Recent low-temperature experiments have reported "satellite" peaks in the current-voltage characteristics of DBRT devices for applied voltages $\approx 70-140$ mV above the main resonance peaks.[10,11] It has been suggested that these satellite peaks are produced when electrons tunnel nonresonantly into the double-barrier device, drop into the resonant state by emitting an optical phonon, and tunnel out through the second barrier.[12]

To calculate the effect of this and other electron–LO-phonon interactions on the current, most researchers use the Frölich interaction approach, which relies on the calculation of a matrix element $\langle f|H_{Fr}|i\rangle$, where H_{Fr} is the Frölich Hamiltonian and the initial and final states $|i\rangle$ and $|f\rangle$ are product states describing the electronic and phonon configurations. The detailed form of the Frölich Hamiltonian in DBRT structures is a matter of some debate since LO phonons can be confined in well or barrier layers.[5,6,13] Interface modes[5] are also possible, but are not considered further in this paper. Although a precise description of confined modes requires a microscopic molecular-dynamics treatment, a good approximate picture for confined modes is obtained using the dielectric continuum model.[14–16] In this picture, LO phonons are confined fully in the well due to differing dielectric properties of barrier and well layers. The electrostatic potential generated by these phonons is of the form $\phi(z)\propto\sin(n\pi z/d)$ with $n=1,2,3,\ldots$ in the confinement area $0<z<d$, and identically zero outside this region. Note that these modes have a potential which is continuous at boundaries, although the corresponding ionic displacement field $u\propto\partial\phi/\partial z\propto\cos(n\pi z/d)$ is discontinuous. For this reason, some authors[6,17] have proposed an alternative continuum picture which employs hydrodynamic boundary conditions; in this case, the phonon displacement field is of the form $u\propto\sin(n\pi z/d)$ with $n=1,2,3,\ldots$ and is continuous at boundaries while the electrostatic potential $\phi(z)\propto\cos(n\pi z/d)$ is discontinuous.

In this paper we study how the spatial structure of the initial and final electronic wave functions Ψ_i and Ψ_f affects the electron-phonon interaction when we consider confined modes of either type discussed above. The form of the wave functions can strongly affect what types of confined LO phonons are emitted as well as the overall strength of the coupling between the electrons and phonons. Two particularly important questions are the following: (i) are confined modes in the barrier layers or the well layers more likely to be emitted, and (ii) is the lowest-order mode, i.e., $n=1$, always the most likely for emission or can higher order modes—e.g., $n=2$—dominate?

Although sophisticated methods have been developed

 ©1991 The American Physical Society

to treat electron-phonon interactions in quantum wells using a quantum transport approach,[1] these methods tend to be practically unwieldy, even without the additional complication of confined versus simple bulk phonon modes. Thus a simpler technique which captures the essential features of the electron-confined phonon interaction and can be easily performed on a microcomputer will be useful for interpreting experimental phonon-assisted tunneling data and designing new experimental structures.

In this paper we use a transfer-matrix approach[18] to obtain the electron transmission probability through $GaAs/Al_xGa_{1-x}As$ DBRT devices and also adapt this method for finding the spatial dependence of the electronic wave function. Section II outlines the method and presents results for the transmission probability and coherent scattering phase shift versus incident electron energy as well as current-voltage characteristics in the absence of any inelastic scattering. In Sec. III we present numerical results showing the spatial dependence of wave functions of selected energies inside the double-barrier structure. The focus is on those spatial properties which affect the electron coupling to the various confined phonon modes (i.e., with $n=1,2,3\ldots$). In particular, we find that for energies off resonance the wave functions show significant spatial symmetry with respect to the GaAs well center. This asymmetry is quantified in Sec. IV with the introduction of an asymmetry parameter δ. In Sec. V we give a formula for the excess current due to phonon-assisted tunneling and discuss qualitative features of this process. Finally, in Sec. VI we numerically calculate matrix-element integrals which describe the electron–LO-phonon interaction in DBRT structures when the phonons are confined and suggest how these may be interpreted experimentally.

Throughout the paper, numerical results are presented for two different $GaAs/Al_xGa_{1-x}As$ devices. Device A has two 30-Å undoped $Al_{0.8}Ga_{0.2}As$ barriers surrounding a 60-Å undoped GaAs well and was selected because it is equivalent to DBRT samples currently being studied in experiments focusing on phonon-assisted tunneling effects.[19] Device B has two 40-Å undoped $Al_{0.45}Ga_{0.55}As$ barriers surrounding an 80-Å undoped GaAs well and is more representative of DBRT structures studied in previous experiments. The numerical results reported here were obtained on a microcomputer with a computational accuracy of eight decimal places.

II. TRANSMISSION PROBABILITY ACROSS DOUBLE-BARRIER STRUCTURES

We assume for the DBRT structure that the potential-energy function varies in the z direction only. Using the effective-mass approximation, we then separate the three-dimensional single-electron Schrödinger equation into parts which are transverse and parallel to the device layers. The total electron energy E_{tot} is then written as the sum of these parallel and transverse components:

$$E_{tot}=E+\hbar^2|\mathbf{k}_{\parallel}|^2/2m^* , \tag{2.1}$$

where $\mathbf{k}_{\parallel}$ is the wave vector in the x-y plane parallel to the $GaAs/Al_xGa_{1-x}As$ interfaces, and E denotes the electron kinetic energy perpendicular to the interfaces (i.e., in the z direction). The total wave function can then be expressed as a product:

$$\Psi(x,y,z)=\frac{1}{\sqrt{A}}e^{i\mathbf{k}_{\parallel}\cdot\mathbf{r}_{\parallel}}\varphi(z) , \tag{2.2}$$

where A is the area of the device, $\mathbf{k}_{\parallel}$ and $\mathbf{r}_{\parallel}$ are vectors in the x-y direction, and φ is a solution to the following one-dimensional Schrödinger equation:[20]

$$\frac{-\hbar^2}{2}\frac{d}{dz}\left[\frac{1}{m^*(z)}\right]\frac{d\varphi}{dz}+U(z)\varphi=E\varphi . \tag{2.3}$$

Here $m^*(z)$ denotes the position-dependent electron (band gap) effective mass and $U(z)$ is the potential seen by a single electron, which includes effects of both conduction-band discontinuities at $GaAs/Al_xGa_{1-x}As$ interfaces and external applied voltage. A typical graph of $U(z)$ is shown in Fig. 1. The conduction-band offset, effective mass, and dielectric constant in each region of the DBRT structure are determined as functions of the aluminum concentration x by the following standard approximations:[21]

$$\Delta E_c=\begin{cases}0.75x \text{ eV for } 0\le x\le 0.45\\ 0.75x+0.69(x-0.45)^2 \text{ eV for } 0.45<x\le 1 ,\end{cases} \tag{2.4}$$

$$m^*/m_0=0.067+0.083x \quad \text{for } 0\le x\le 1 , \tag{2.5}$$

and

$$\epsilon/\epsilon_0=13.1-3.0x \quad \text{for } 0\le x\le 1 . \tag{2.6}$$

Ignoring accumulation and depletion effects,[22] the voltage drop in each section is given by

$$V_1=\frac{d_1}{2(\epsilon_1/\epsilon_2)d_2+d_1}V , \tag{2.7}$$

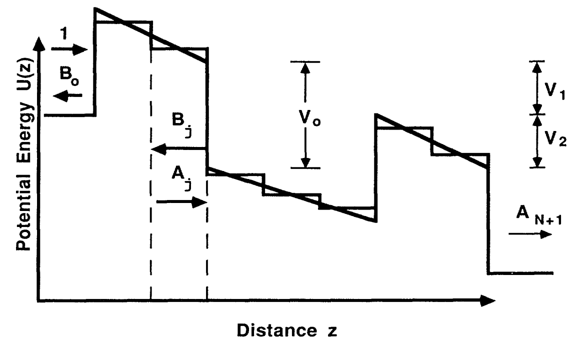

FIG. 1. Schematic drawing of the exact potential $U(z)$ for a double-barrier structure and the step approximation used in transfer matrix calculations. Device A has parameters $d_1=60$ Å, $d_2=30$ Å, and $V_0=684$ meV. Device B has parameters $d_1=80$ Å, $d_2=40$ Å, and $V_0=338$ meV. V_0 is the conduction-band-edge discontinuity.

$$V_2=\frac{(\epsilon_1/\epsilon_2)d_2}{2(\epsilon_1/\epsilon_2)d_2+d_1}V\ , \tag{2.8}$$

where V is the total applied voltage, ϵ_1 is the dielectric constant in the GaAs well region, and ϵ_2 is the dielectric constant in the $Al_xGa_{1-x}As$ barrier region.

To solve for the transmission probability, we use a transfer-matrix method similar to one presented, for example, by Ando and Itoh.[18] This method, in which the exact potential is approximated by a series of steps (see Fig. 1), has among its advantages computational simplicity and good accuracy. In fact, Ando and Itoh[18] have shown—and we have reconfirmed here—that as the number of steps increases, the solution rapidly converges to a single result. For double-barrier structures of the type considered here and under low bias (<1.0 V), 15 steps for the entire structure is generally sufficient to ensure excellent convergence.

Because the potential is treated as constant over each step, the solution to the one-dimensional Schrödinger equation is given in the jth step as a superposition of plane waves:

$$\varphi_j(z_j)=A_je^{k_jz_j}+B_je^{-k_jz_j}\ , \tag{2.9}$$

with the z component of the complex wave vector k_j given by

$$k_j=\left[\frac{2m_j^*(U_j-E)}{\hbar^2}\right]^{1/2}\ , \tag{2.10}$$

and $J=0,1,2,\ldots,N,N+1$ for a total of $N+1$ steps. Here U_j and m_j^* are the potential and effective mass associated with step j, and z_j is distance measured from the left-hand side of the jth step. Furthermore, the steps are all assumed to have the same length a and the j values increase as the structure is traversed from left to right (see Fig. 1). Our method differs from the previous one of Ando and Itoh[18] in that we use a separate coordinate system for each step. This simplifies the form of the equations which follow and ensures that arguments of the exponentials—i.e., $\pm k_jz_j$—are small, giving improved numerical accuracy.

Imposing continuity of the wave function φ and its appropriately normalized derivative $(1/m^*)(d\varphi/dz)$ at the boundary between steps j and $j+1$, one derives a matrix formula that relates the successive A and B plane-wave coefficients, namely,

$$\begin{bmatrix}A_{j+1}\\B_{j+1}\end{bmatrix}=\underline{M}_j\begin{bmatrix}A_j\\B_j\end{bmatrix}\ , \tag{2.11}$$

where

$$\underline{M}_j=\frac{1}{2}\begin{bmatrix}(1+r_j)e^{k_ja} & (1-r_j)e^{-k_ja}\\(1-r_j)e^{k_ja} & (1+r_j)e^{-k_ja}\end{bmatrix} \tag{2.12}$$

and

$$r_j=\frac{m_{j+1}^*k_j}{m_j^*k_{j+1}}\ . \tag{2.13}$$

The $\underline{M}_j$ matrices are then multiplied together to relate the plane-wave coefficients A_0 and B_0 in the emitter layer to the coefficients A_{N+1} and B_{N+1} in the collector layer:

$$\begin{bmatrix}A_{N+1}\\B_{N+1}\end{bmatrix}=\underline{M}_{\rm tot}\begin{bmatrix}A_0\\B_0\end{bmatrix}\ , \tag{2.14}$$

with

$$\underline{M}_{\rm tot}\equiv\begin{bmatrix}M_{11} & M_{12}\\M_{21} & M_{22}\end{bmatrix}=\underline{M}_N\cdots\underline{M}_1\underline{M}_0\ . \tag{2.15}$$

Setting $A_0=1$ and $B_{N+1}=0$ in Eq. (2.14)—which physically corresponds to an electron incident from the left-hand side of Fig. 1 and generates *left-justified* states—we arrive at the following simple expression for the transmission amplitude A_{N+1}:

$$A_{N+1}\frac{k_0}{k_{N+1}}\left[\frac{1}{M_{22}}\right]\ , \tag{2.16}$$

where we have used the relation $\det(\underline{M}_j)=r_j$, which in turn leads to $\det(\underline{M}_{\rm tot})=k_0/k_{N+1}$ (note that the effective-mass factors cancel because the collector and emitter layers have identical material composition).

The transmission probability P is now defined as the ratio of the transmitted particle flux divided by the incident particle flux[23] and depends on both the incident electron energy E and the applied voltage V. This definition leads directly to the following simple expression:

$$P(E;V)=\frac{|k_{N+1}|}{|k_0|}|A_{N+1}|^2\ . \tag{2.17}$$

Figure 2(a) shows a numerical calculation of this transmission probability versus incident electron energy for device A with zero applied voltage. Sharp peaks occur in the transmission for the resonant energies $E_1=77.14$ meV and $E_2=313.62$ meV, the energies of the ground and first excited *quasibound* states of the GaAs well. As predicted for a potential structure which is symmetric about the well center, $P(E;0)$ has a peak value of 1.0 at each resonance, corresponding to complete transmission.[24]

Figure 2(b) shows a plot of transmission probability versus applied voltage for the same structure with the incident electron energy fixed at 1 meV. In this case the potential is no longer symmetric; thus the transmission probability no longer achieves a peak value of 1.0.[24] Otherwise, the P vs E and P vs V curves are remarkably similar, with successive peaks in the latter (at 0.150 and 0.639 V, respectively) occurring at applied potentials which are roughly twice the corresponding peak values for the P vs E curve. This is reasonable as the potential-energy drop at the center of the GaAs well is one-half the total applied potential drop, and because the applied voltages are low enough so that tunneling properties of the potential structure are relatively unaffected. To summarize, we find for device A that varying the energy of the incoming electrons with fixed voltage and varying the applied voltage for fixed incident energy both lead to qualitatively

similar transmission curves. Behavior of device B is also qualitatively similar under voltage or electron-energy variation.

Another important property of coherent transport through the DBRT structure is the scattering phase shift of the transmitted electron, given by $\alpha=\tan^{-1}[\mathrm{Im}(\varphi_{N+1})/\mathrm{Re}(\varphi_{N+1})]$. Figure 3(a) shows the phase shift α as a function of incident electron energy for device A with no applied voltage. For most of the energy range the phase shift gradually increases; however, around resonance it rapidly shifts through 180°. The abruptness of this shift is shown in Fig. 3(b), where α is plotted for energies very near the ground-state resonance. As expected, the width of the step (approximately 0.03 mev in this case) corresponds to the characteristic resonance width of transmission curve in Fig. 2(a).

The phase shift α may be related to the time delay $\Delta\tau$ experienced by a wave packet through the approximation $\Delta\tau\approx\hbar\, d\alpha/dE$.[20,25] For most energies the time delay is rather small, but near resonance the wave packet spends significantly more time in the DBRT structure.[26–28] One effect of these time delays may be to enhance certain types of inelastic scattering—e.g., the interaction with confined phonons—near resonance.

Once the transmission probability is obtained, the current density through the structure is calculated using the Tsu-Esaki current formula[4]

$$J=\frac{em^*k_BT}{2\pi^2\hbar^3}\times\int_0^\infty P(E;V)\ln\left[\frac{1+\exp(E_F-E)/k_BT}{1+\exp(E_F-E-eV)/k_BT}\right]dE\ , \tag{2.18}$$

where E_F is the Fermi energy, T is the temperature, E is the electron kinetic energy transverse to the device layers, k_B is the Boltzmann constant, and m^* is the electron effective mass in GaAs.

Figure 4(a) shows a plot of the current density J vs applied voltage V for device A with $E_F=20$ meV (corresponding to a doping in the emitter layer of roughly 2×10^{17} cm^{-3}) and $T=4$ K. The current peaks at approximately 0.15 and 0.6387 V, the same voltages as the transmission resonance peaks in Fig. 2(b). Because the transmission peaks are very narrow ($\approx3\times10^{-5}$ eV for the ground state) and the thermal energy is small ($\approx3\times10^{-4}$ eV), the observed width of the current peaks is determined entirely by the energy bandwidth of the Fermi distribution in the emitter layer which, at low temperatures, is simply the Fermi energy E_F. This is important if one wants to separate out the effects of phonon-assisted tunneling satellite peaks[10] from the principal resonant tunneling peaks in experimental I-V curves. In order to observe distinct satellite peaks we need to have principal current peak widths which are less than the characteristic LO-phonon energies. We note that if space-charge depletion and accumulation effects are important (as can occur, e.g., when undoped GaAs spacer

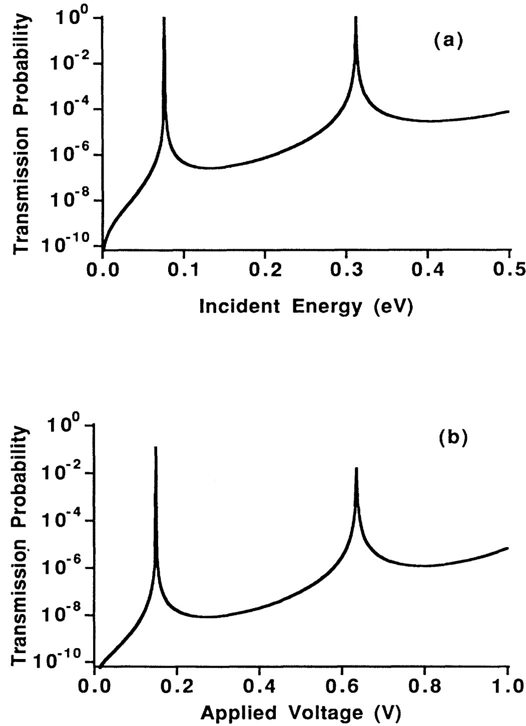

FIG. 2. (a) Transmission probability vs energy for device A with no applied voltage. The transmission peaks are centered on 77.135 and 313.61 meV. (b) Transmission probability vs *applied voltage* for the same structure with fixed incident energy $E=1$ meV. The transmission peaks occur at 0.15 and 0.64 V.

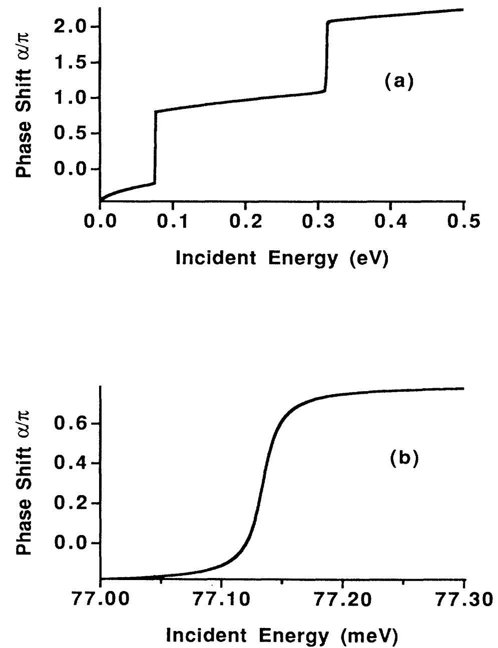

FIG. 3. (a) Coherent scattering phase shift vs energy for device A. (b) Phase shift vs energy near the ground-state resonance.

layers are included in the DBRT structure,[11]) they may also affect widths of current peaks.

As the temperature increases to $T=77$ K in Fig. 4(b), the Fermi distribution in the emitter layer broadens, washing out the left-hand side of the current peaks. However, the right-hand side of the peaks remains abrupt on the scale of the transmission resonance widths. As stated above, these calculations have ignored effects of incoherent electron scattering, space-charge effects, and more complicated many-electron effects, all of which can be important in certain real devices. As a result, typical experimental *I-V* curves for DBRT structures only qualitatively resemble the graphs in Fig. 4.

III. SPATIAL STRUCTURE OF ELECTRONIC WAVE FUNCTIONS

Once the transmitted wave amplitude A_{N+1} is found using Eq. (2.16), the left-justified electronic wave function can be calculated across the entire DBRT structure by inverting the $\underline{M}_j$ and then successively solving for the A_j and B_j according to

$$\begin{bmatrix} A_j \\ B_j \end{bmatrix} = \underline{M}_j^{-1} \begin{bmatrix} A_{j+1} \\ B_{j+1} \end{bmatrix} , \tag{3.1}$$

where

$$\underline{M}_j^{-1} = \frac{1}{2} \begin{bmatrix} (1+1/r_j)\exp(-k_j a) & (1-1/r_j)\exp(-k_j a) \\ (1-1/r_j)\exp(k_j - a) & (1+1/r_j)\exp(k_j a) \end{bmatrix} . \tag{3.2}$$

Four plots of $|\varphi|^2$ at successively increasing electron energies are shown in Figs. 5(a)–5(d) for device *A*. In these log-linear plots, $|\varphi|^2$ is shown as a function of transverse position z over the entire double-barrier structure. In Fig. 5(a), with the incident electron energy below the first resonance, $|\varphi|^2$ behaves as expected: in the barrier regions the wave function decays exponentially, while in the well region the wave function is roughly constant. Figure 5(b), a plot for the ground-state resonant energy $E=77.135$ meV, is also consistent with theoretical predictions.[24] In particular, $|\varphi|^2$ is a *symmetric* function about the well center and strongly peaked there, so that the effective electron density in the well is enhanced by approximately three orders of magnitude relative to the incident wave amplitude.

In studying phonon-assisted tunneling, we expect that the spatial behavior and overlap of the initial and final-

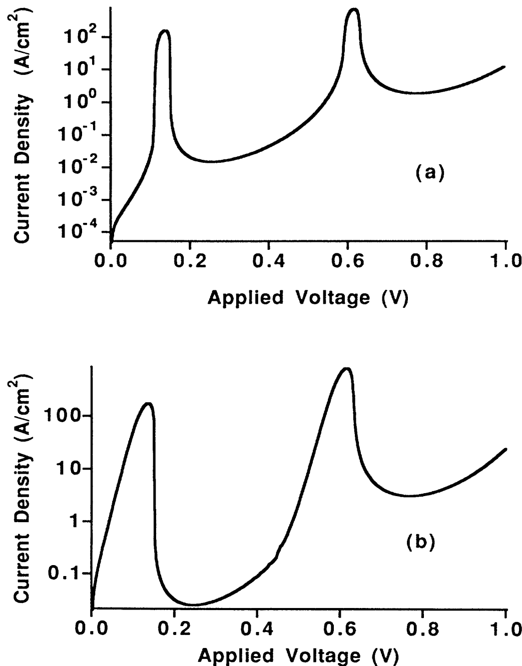

FIG. 4. (a) Current density vs applied voltage $J(V)$ for device *A* with Fermi energy $E_F=20$ meV and temperature $T=4$ K. (b) $J(V)$ for the same structure at temperature $T=77$ K.

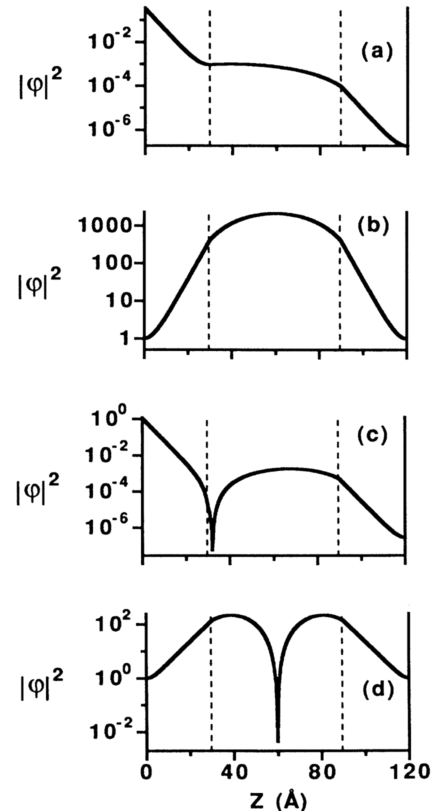

FIG. 5. Spatial dependence of $|\varphi|^2$ throughout device *A* with zero bias for electron energies: (a) $E=50.000$ meV, (b) $E=77.135$ meV, (c) $E=113.135$ meV, and (d) $E=313.610$ meV.

state wave functions will play an important role. For the important case of LO-phonon emission in the z direction, the final state is taken to be the resonant state at $E=77.135$ meV and the initial state has energy $E=77.135$ meV$+\hbar\omega_0$, where $\hbar\omega_0$ is the LO-phonon energy. Because the LO-phonon energy in GaAs is approximately 36 meV, the wave function plotted in Fig. 5(c) is for an energy $E=113$ meV, that is, 36 meV above the ground-state energy. It is important to note that the wave function is now visibly asymmetric with respect to the well center [the cusplike dip in Fig. 5(c) is simply a zero of the wave function as plotted on a logarithmic scale]. Finally, a plot of the first excited resonant state at $E=313.62$ meV is shown in Fig. 5(d). It exhibits a large enhancement of electron density in the well as for the ground state, although there is now a sharp dip indicating a wave-function mode at the well center. This results from the fact that the first excited state is spatially *antisymmetric* with respect to the well center.[29]

An equivalent set of wave-function plots is shown in Fig. 6 for device B with no applied voltage. Although Figs. 5 and 6 differ quantitatively, their essential features are the same. Off resonance, the wave functions of Figs. 6(a) and 6(c) decay in the barrier layers from left to right, while the ground and first excited-state wave functions—in Figs. 6(b) and 6(d)—are strongly peaked in the well and exhibit the same symmetry properties observed for device A. The nonresonant states—particularly those of Figs. 5(c) and 6(c)—show significant asymmetry which, when quantified below, is of a similar order of magnitude for either device A or B. In addition to devices A and B, we have numerically studied the spatial dependence of wave functions in several other relatively narrow DBRT structures with differing Al barrier layer concentrations and layer thicknesses, and have found that they all share these general features.

To better see the symmetric and asymmetric behaviors of the resonant and nonresonant states we have replotted in Fig. 7 the wave functions of Fig. 5 in the well region using a linear scale. Clearly visible in Figs. 7(a) and 7(c) is the strong lack of symmetry with respect to center of the GaAs well. This behavior has important consequences for the relative magnitudes of the electron-phonon matrix elements discussed in Sec. VI.

We have also examined the spatial dependence of wave functions when the applied voltage is varied and the incident energy is fixed and we find behavior which is qualitatively similar to that observed above for fixed voltage and variable incident energy. Again, the wave function is strongly peaked in the well on resonance, and for an ap-

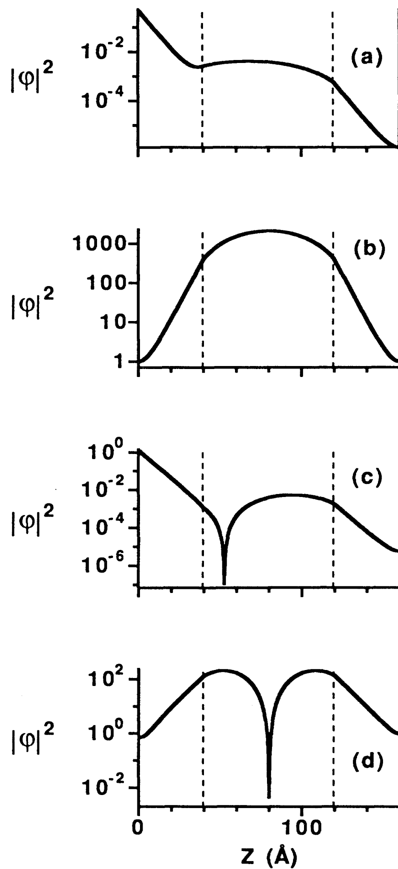

FIG. 6. Spatial dependence of $|\varphi|^2$ throughout device B with no applied voltage and electron energies: (a) $E=30.00$ meV, (b) $E=44.44$ meV, (c) $E=80.44$ meV, and (d) $E=176.00$ meV.

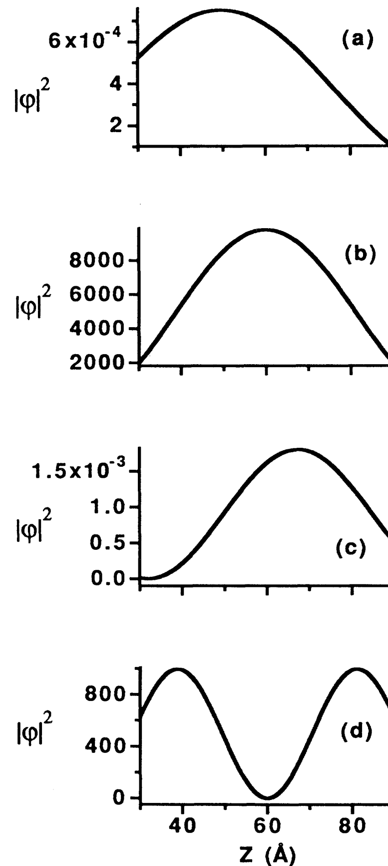

FIG. 7. Spatial dependence of $|\varphi|^2$ in the well region of device A for electron energies: (a) $E=50.00$ meV, (b) $E=77.135$ meV, (c) $E=113.135$ meV, and (d) $E=313.620$ meV.

plied voltage 2(36 meV)/e=72 mV above the resonant value, the wave function shows significant asymmetry with respect to the well center. We find that this asymmetry is of a similar order of magnitude for either fixed energy conditions or the zero voltage bias conditions discussed above. Additionally, we find that the ground and first excited states have approximate spatial symmetry behavior about the well center, but not the exact symmetry observed for zero voltage bias because the DBRT potential structure is no longer perfectly symmetric about the well center.[24] We have found that this similarity between spatial behavior versus voltage or versus incident energy holds for applied voltages up to the order of 1 V.

IV. WELL ASYMMETRY PARAMETER

In order to quantify the degree of asymmetry in the GaAs well with respect to the well center, we now define a quantity δ, which can be termed a "well asymmetry parameter." For an electronic wave function φ the parameter δ is defined by

$$\delta=\frac{2}{d_1\eta}\left\langle\varphi\left|\left[z-\frac{d_1}{2}\right]\right|\varphi\right\rangle_w , \tag{4.1}$$

where the integral implied in Eq. (4.1) extends only over the GaAs well from $z=0$ to d_1, and η is the standard normalization: $\langle\varphi|\varphi\rangle_w$. Physically, this parameter is just the normalized first moment of the electron probability distribution $|\varphi|^2$ restricted to the well and relative to the well center at $z=d_1/2$. The well asymmetry parameter δ is plotted versus incident energy in Fig. 8 for device A with no applied voltage. As expected, δ passes through zero as the energy sweeps through the ground and first excited-state resonances; this behavior reflects the exact symmetry of these states.[24] Also visible in Fig. 8 is the fact that δ attains its maximum value of $\sim$30% for an electron energy $\sim$150 meV; this is $\sim$73 meV in excess of the first transmission peak. For an incident energy of 109 meV, which is approximately one optical-phonon energy ($\sim$36 meV) above the ground-state resonance, we find that $\delta\sim$22%. Thus we confirm that the electronic wave functions that couple to the ground state through confined LO-phonon emission are strongly asymmetric.

Other DBRT structures that we have studied share these general features. We generally observe an absolute maximum in the asymmetry parameter δ for energies 40–120 meV above the ground-state value with maximum value typically of the order of 30%. DBRT structures with relatively wider GaAs wells generally exhibit a smaller maximum value of δ as well as a smaller value of δ at 36 meV about the ground state. This will reduce the δ value for nonresonant states with energy on LO-phonon energy $\hbar\omega_0$ in excess of the ground-state energy, which are exactly the states that lead to phonon-assisted tunneling in I-V curves at low temperature. On the other hand, lower $Al_xGa_{1-x}As$ barrier heights (i.e., those with smaller Al concentration) tend to slightly *increase* the maximum asymmetry as well as the asymmetry at one phonon energy above the ground state. Thus we anticipate that processes which are sensitive to wave-function asymmetry such as electron–confined–phonon scattering with the lowest-order phonon mode ($n=1$), should be more readily observable in wide DBRT structures that also have large x values. On the contrary, if we want to suppress this type of scattering, the trend should be towards narrower DBRT structures with smaller x values (although not x so small that the phonons are no longer confined[13]).

For a nonzero applied voltage, the δ vs E and P vs E curves both shift downward in energy, but other features are qualitatively similar to the case of zero applied voltage. This behavior is shown in Fig. 9, which plots the well asymmetry parameter and transmission probability for device A with a fixed applied voltage V=0.1 V. In this case the effect of the applied bias is to slightly increase the maximum value of asymmetry to $\sim$33%; also, the energy value for which maximum δ occurs is approximately 65 meV in excess of the ground-state resonant energy, a smaller energy separation than that which occurs for the same device when unbiased. Furthermore, for an incident energy of 66 meV—approximately one optical-phonon energy above the ground-state resonance—we find $\delta\sim$27%, which implies that the effect of applied voltage is to increase the asymmetry of electronic wave functions which couple to the ground state via confined LO-phonon emission. We have confirmed these trends in other DBRT devices at several different applied voltages

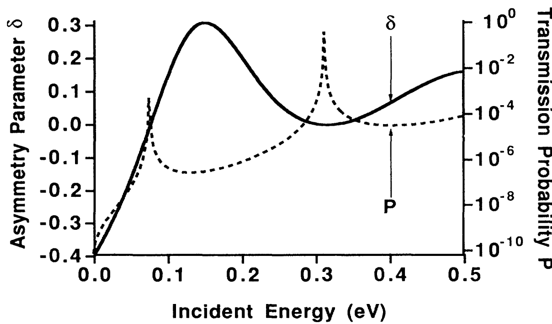

FIG. 8. Well asymmetry parameter $\delta(E)$ and corresponding transmission probability $P(E;V)$ for device A with zero applied bias.

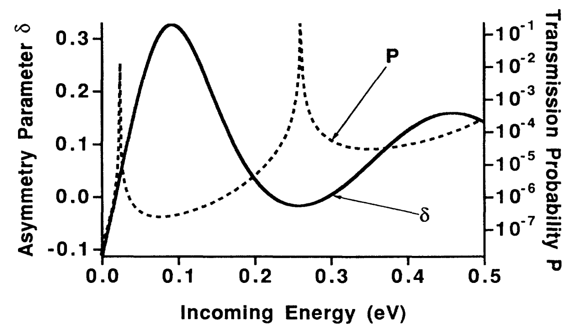

FIG. 9. Well asymmetry parameter $\delta(E)$ and corresponding transmission probability $P(E;V)$ for device A with an applied voltage of 0.1 V.

and find that maximum asymmetry parameters as high as 45% can be achieved for appropriately designed structures.

V. PHONON-ASSISTED TUNNELING

Several experiments have observed satellite peaks in DBRT current at voltages just above the resonant peak and have attributed these peaks to phonon-assisted tunneling.[10,11] At these voltages a small but finite portion of the emitter electronic wave function extends through the DBRT structure, as we have seen above. This wave function can couple with the resonant state through the emission of a LO phonon. If the width of the Fermi sea of electrons is less than the phonon energy and the experiment is performed at low temperatures, then the resonant state energy will be less than energy of the conduction-band edge. Therefore every electron that drops into the resonant state can only tunnel out through the collector barrier resulting in measurable current.

To calculate the excess current due to phonon-assisted tunneling we first consider what types of electronic states will contribute to the current. In a DBRT structure with emitter and collector contacts, we can create two types of orthogonal electronic states. Left-justified states, the kind we have considered here, are formed by an incident plane wave incident from the emitter. Right-justified states are formed by plane waves incident from the collector. The phonon-assisted tunneling process is illustrated in Fig. 10 for a specific incident electron energy, and it is easy to see that the initial wave function for phonon-assisted tunneling will be composed only of left-justified states. Right-justified states can enter the well and emit a phonon, but once the electron has dropped into the resonant state it can only tunnel back out through the collector barrier. Thus the contribution of right-justified states to the current will be zero.

On the other hand, since the energy of the final state is lower than the conduction-band edge energy in the emitter, the final (resonant) state for phonon-assisted tunneling can only be a right-justified state. When the width of the resonant state is relatively narrow it is generally reasonable to approximate the final state as a fully confined state in the well.[12] For the DBRT structures considered here this approximation is quite good.

The excess current density due to phonon-assisted tunneling can then be calculated using

$$J=\frac{1}{A}\int eW_{\text{con}}(\mathbf{k})g_e(\mathbf{k})f_e(E(\mathbf{k}))d\mathbf{k}\ , \tag{5.1}$$

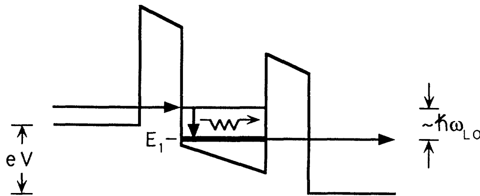

FIG. 10. Schematic illustration of phonon-assisted tunneling in a DBRT structure under applied voltage V. The emitted phonon is assumed to have negligible momentum parallel to the interfaces.

where $g_e(\mathbf{k})=2AL_e/(2\pi)^3$ is the density of states in the emitter, $f_e(\mathbf{k})$ is the Fermi distribution of carriers in the emitter, AL_e is the effective volume of the emitter, and $W_{\text{con}}(\mathbf{k})=\sum_f W(i\to f)$ is the *total* phonon emission rate per electron from a given initial emitter state with wave vector $\mathbf{k}$. The sum $\sum_f$ is over all final states which have a z component of energy equal to that of the resonant state. Equation (5.1) is heuristically justified by noting that there are $f_e(\mathbf{k})g_e(\mathbf{k})$ emitter electrons per unit volume of $\mathbf{k}$ space which tunnel by confined phonon emission into the collector at a rate per electron $W_{\text{con}}(\mathbf{k})$. To obtain the total phonon-assisted tunneling current we simply multiply these factors by the electronic charge and integrate over $\mathbf{k}$ space.

The scattering rate $W(i\to f)$ is calculated using the Fermi golden rule:

$$W(i\to f)=\frac{2\pi}{\hbar}|\langle f|\mathcal{H}_{\text{Fr}}|i\rangle|^2\delta(E_i-E_f-\hbar\omega_0)\ , \tag{5.2}$$

where E_i is the energy of the initial electronic state, E_f is the energy of the final electronic state, $\hbar\omega_0$ is the energy of the emitted LO phonon, and $\mathcal{H}_{\text{Fr}}$ is the Frölich Hamiltonian. Note that the states $|f\rangle$ and $|i\rangle$ are direct product states of the electronic and phonon wave functions.

As stated in the Introduction, the exact form of the Fröhlich interaction due to confined phonon modes in DBRT structures is not known. Two widely used models are the dielectric continuum model[5] and the hydrodynamic continuum model.[6] In both of these models, $\mathcal{H}_{\text{Fr}}$ can be written as

$$\mathcal{H}_{\text{Fr}}^{\text{con}}=\sum_{\mathbf{q}_\parallel,n}\gamma\frac{1}{[q_\parallel^2+(n\pi/d)^2]^{1/2}}e^{i\mathbf{q}_\parallel\cdot\mathbf{r}_\parallel}\times f(z,n)[a_n(\mathbf{q}_\parallel)+a_n^\dagger(-\mathbf{q}_\parallel)]\ , \tag{5.3}$$

where

$$\gamma=\left[\frac{\hbar\omega_0 e^2}{AL_e\epsilon_0}\left[\frac{1}{\kappa_\infty}-\frac{1}{\kappa_0}\right]\right]^{1/2}. \tag{5.4}$$

The electrostatic potential associated with the phonons is given by

$$f(z,n)=\sin\left[\frac{n\pi}{d}\right] \tag{5.5}$$

for the dielectric continuum model, or

$$f(z,n)=\cos\left[\frac{n\pi}{d}\right] \tag{5.6}$$

for the hydrodynamic continuum model. In these formulas, $\mathbf{q}_\parallel$ is the wave vector of the emitted phonon in the x-y plane, $a_n^\dagger(\mathbf{q}_\parallel)$ and $a_n(\mathbf{q}_\parallel)$ are the creation and annihilation operators for phonons, ϵ_0 is the permittivity of free space, κ_∞ and κ_0 are the high- and low-frequency relative dielectric constants, respectively, $\hbar\omega_0$ is the energy of LO phonons, and d is the width of the confining region, either the well or the barrier. When this Hamiltonian is substituted into the Fermi golden rule, Eq. (5.2), the resulting emission rate is easily shown to be

$$W(i\to f)=\frac{2\pi\alpha^2P_n^2}{\hbar\left[\left[\frac{n\pi}{d}\right]^2+q_\parallel^2\right]}\times\delta_{\mathbf{k}_\parallel-\mathbf{k}'_\parallel-\mathbf{q}_\parallel}\delta(E_i-E_f-\hbar\omega_0)\ , \qquad (5.7)$$

where the overlap integrals of the electronic states with the phonon potentials are given by

$$P_n=\int_0^d\varphi_f^*(z)\sin\left[\frac{n\pi z}{d}\right]\varphi_i(z)dz$$

$$\text{(dielectric continuum model)}\ , \qquad (5.8)$$

$$P_n=\int_0^d\varphi_f^*(z)\cos\left[\frac{n\pi z}{d}\right]\varphi_i(z)dz$$

$$\text{(hydrodynamic continuum model)}\ . \qquad (5.9)$$

The rate in Eq. (5.7) must then be summed over the final states in the parallel direction to calculate the total emission rate $W_{\text{con}}(\mathbf{k})$. This emission rate has several important properties. First of all, it is largest when $q_\parallel \ll n\pi/d$, i.e., when the emitted phonon has very little momentum in the x-y plane and most of the electron-energy loss is in the z direction,[30] a tendency which is generally confirmed by experiments in bulk materials.[31,32] Thus most of the phonon-assisted tunneling current arises from initial electronic states that have a z component of energy that is $\sim\hbar\omega_0$ above the resonant state energy. Second, when $q_\parallel$ is small, we have found that $W_{\text{con}}(\mathbf{k})$ is only a weak function of $\mathbf{k}_\parallel$, where $\mathbf{k}_\parallel$ is the incoming electron momentum in the x-y plane.[30] Thus we have the following useful approximation for the total emission rate:

$$W_{\text{con}}(\mathbf{k},n)\propto\frac{P_n^2}{\left[\frac{n\pi}{d}\right]^2}\equiv Q_n\ . \qquad (5.10)$$

We could also deduce this expression directly from Eq. (5.7) simply by noting that the terms for which $W(i\to f)$ is maximum have $q_\parallel\approx 0$.

Although the precise calculation of $W_{\text{con}}(\mathbf{k})$ can be a somewhat complicated procedure, the relative strength of the satellite peaks due to phonon-assisted tunneling can be approximately determined using Eq. (5.10). In particular, satellite current peaks are expected to be directly proportional to the Q_n's. We choose an initial state that has a z component of electronic energy that is $\hbar\omega_0$ above the resonant value since these are the states that will contribute most strongly to the phonon-assisted tunneling current. Then, using Eq. (5.10), we can determine whether phonons are emitted preferentially in the barrier layers or the well, and which type of model for the confined phonons—the hydrodynamic or the dielectric continuum—will give the larger excess current. The comparisons will only be approximate, but they are much easier to perform than the direct current calculations and give a useful guide to the relative importance of different types of confined phonon scattering in measured current voltage curves.

VI. MATRIX-ELEMENT CALCULATIONS

We have numerically calculated the Q_n from Eq. (5.10) in the dielectric continuum for the GaAs well of device A using confined phonons with mode numbers $n=1,2,3$, and the results are displayed in Table I. In the first line of the table we calculate the Q_n where φ_f is the ground state with energy 77.1352 meV and the initial state φ_i has energy 113.1352 meV, one GaAs optical-phonon energy in excess of the ground-state value. The length of the confining region d is measured in angstroms, and the factor L_e that arises from the normalization of the incoming electronic state has been removed. In the full calculation of current, Eq. (5.1), the factor L_e cancels with an identical factor in the density of states. Note that Q_1 is the largest of the three, indicating that the emission of a phonon with $n=1$ is the most likely. The second line of Table I displays the Q_n where φ_f is now the first excited state with energy 313.6137 meV and the initial state has energy 349.6137 meV, again assuming 36-meV LO-phonon energies. Note that the emission of an $n=3$ phonon has been considerably enhanced by the different spatial properties of the first excited state.

The third and fourth lines of Table I presents calculations of the Q_n for the left-hand $Al_xGa_{1-x}As$ barrier.[33] For x values greater than 0.7, the LO phonons in Al_xGa_{1-x} are primarily AlAs-like,[34] with an energy of 50.1 meV. As a result, in the first row of Table I we calculate the Q_n where the initial state φ_i has an energy of 127.2352 meV, 50.1 meV about the ground-state value, while the second row presents calculations of the Q_n where φ_i has energy of 363.7137 meV, 50.1 meV above the first excited state. In both cases the $n=1$ mode dominates the higher-order modes.

We have numerically calculated the Q_n in the hydrodynamic continuum model for the well and barrier of device A with confined phonons of mode numbers 1, 2, and 3, and the results are displayed in Table II. In the first line of the table we calculate the Q_n where φ_f is the

TABLE I. Electron-phonon matrix-element integrals calculated with the dielectric continuum model.

Initial energy (meV)	Final energy (meV)	Layer	$Q_{n=1}$	$Q_{n=2}$	$Q_{n=3}$
113.1352	77.1352	well	1.88×10^{-9}	2.00×10^{-11}	5.07×10^{-14}
349.6137	313.6137	well	2.38×10^{-8}	2.68×10^{-11}	3.48×10^{-9}
127.2352	77.1352	barrier	3.98×10^{-12}	5.45×10^{-15}	5.38×10^{-14}
363.7137	313.6137	barrier	1.24×10^{-10}	2.82×10^{-12}	2.52×10^{-13}

ground-state wave function with energy 77.1352 meV and the initial state φ_i has energy 113.1352 meV, which is one GaAs optical-phonon energy in excess of the ground-state value. The second line of Table II displays the Q_n where φ_f is now the first excited state with energy 313.6137 meV and the initial state has energy 349.6137 meV, again assuming 36-meV LO-phonon energies. For the ground-state resonance Q_1 and Q_2 are approximately the same, indicating that, in contrast with the dielectric continuum model, the $n=2$ and 1 modes will contribute just about equally. This is due to the difference in spatial symmetry properties of phonon potentials in the dielectric versus hydrodynamic continuum models.

The last two lines of Table II present calculations of Eq. (5.10) for the first $Al_xGa_{1-x}As$ barrier. In the third row of Table II we calculate the Q_n where the initial state φ_i has an energy of 127.2352 meV, 50.1 meV above the ground state, while the fourth row presents calculations of the Q_n where φ_i has energy of 363.7137 meV, 50.1 meV above the first excited state. In both cases the $n=1$ mode dominates.

The first thing we note about these tables is the strong effect of electronic state symmetry properties. This follows because phonon-assisted tunneling in DBRT structures does not involve transitions between two subbands or entirely within one subband. Thus, in contrast to calculations of electron-confined phonon interactions in quantum wires,[15] no phonon mode may be excluded on the basis of its symmetry properties alone, and the relative symmetry of the electronic states will thus play a decisive role in determining which phonons are preferentially emitted. This effect is most striking for the hydrodynamic continuum model, as the Q_1 and Q_2 are approximately equal in line 1 of Table II. If phonon-assisted tunneling were either a purely intersubband or intrasubband process, one of these Q_n would be zero.

In both the dielectric and hydrodynamic continuum models, the electron-phonon matrix-element integrals in the well are larger than the corresponding integrals in the barrier for energies near the first resonance of device A. Thus, for the dielectric continuum modes of Table I, the largest Q_n in the well layer with final-state energy $E=77.1352$ meV is about 500 times larger than the largest corresponding Q_n in the barrier layer. Similarly, for the hydrodynamic modes of Table II, the largest Q_n in the well region with final-state energy $E=77.1352$ meV is more than 1000 times larger than the largest corresponding barrier value. This means that, in general, there is a greater probability of emitting a phonon in the well rather than emitting a phonon in the first barrier for energies near the first resonance. This tendency should be even greater in the real case where voltage is applied, since this tends to reduce the magnitude of the final-state wave function in the first barrier. We have verified this behavior in other DBRT structures with design parameters similar to device A—that is, relatively narrow barriers (<50 Å) with relatively large Al concentration ($x>0.6$). As an experimental consequence of preferred phonon emission in the GaAs well, we expect the phonon-assisted tunneling satellite peaks in I-V curves due to confined modes in the well will be substantially larger than satellite peaks due to barrier confined modes.

Current-voltage characteristics may also enable researchers to distinguish between the two types of confined phonon modes referred to above. Note that the electron-phonon matrix-element integrals for the dielectric continuum model tend to be substantially larger than the corresponding integrals for the hydrodynamic continuum model. For instance, comparing the largest elements of the first lines of Tables I and II, we notice that the Q_1 entry in Table I is about 10 times larger than the Q_1 entry in Table II. As a result, the current satellite peaks due to phonon-assisted tunneling are predicted to be approximately 10 times larger for the confined modes of the dielectric continuum model. Detailed numerical calculations of DBRT device current-voltage characteristics which use the Q_n values to predict absolute magnitudes for the satellite peaks are in progress and will be reported in a separate publication.[30]

VII. CONCLUDING REMARKS

In this paper we have numerically examined electronic wavefunctions in $GaAs/Al_xGa_{1-x}As$ DBRT structures. In addition to confirming expected behavior for the transmission coefficient and current density, we have shown that the electronic wave functions for off-resonance energies can be significantly asymmetric with respect to the center of the well. This turns out to have a strong effect on the coupling between electron states and the confined LO phonons in double-barrier quantum well structures.

The sensitivity of spatial properties of electronic wave functions on DBRT device parameters suggests the possibility of "wave-function engineering." Thus, for example, the width of the well and the height of the barriers might be experimentally designed in order to minimize the effect of electron–confined-LO-phonon coupling, or to enhance scattering via one phonon mode over another. The asymmetry of off-resonance electronic wave functions should also have measurable effects on the optical properties of appropriately constructed quantum-well de-

TABLE II. Electron-phonon matrix-element integrals calculated with the hydrodynamic continuum model.

Initial energy (meV)	Final energy (meV)	Layer	$Q_{n=1}$	$Q_{n=2}$	$Q_{n=3}$
113.1352	77.1352	well	9.02×10^{-11}	8.22×10^{-11}	2.79×10^{-13}
349.6137	313.6137	well	5.72×10^{-13}	2.46×10^{-9}	5.05×10^{-11}
127.2352	77.1352	barrier	9.21×10^{-14}	7.69×10^{-15}	3.96×10^{-15}
363.7137	313.6137	barrier	3.26×10^{-11}	6.47×10^{-12}	7.54×10^{-13}

vices.[35]

Throughout this paper, we have neglected various effects that can be significant in determining the *I-V* curves of real devices. A particularly important case concerns space-charge effects in which accumulation and depletion layers may form which take up much of the voltage drop across the device. This, in turn, can create charge buildup in the well and may significantly alter the shape of the potential in the DBRT structure.[11] Such effects tend to be more important in structures that are grown with large spacer layers. While the effect of charge buildup can be quantified with the use of self-consistent calculations, the effect of accumulation and depletion layers is difficult to calculate under the nonequilibrium conditions that result when a current flows through the device.[36] One frequently used approximation involves calculating the voltage drop across accumulation and depletion layers using a static Poisson equation which assumes that the flow of current does not appreciably alter the charge density.[18] Such an approach could be incorporated into our method for calculating phonon-assisted tunneling in a straightforward manner.

If the dielectric continuum picture of localized phonon modes is essentially correct, then an effect which is expected to be particularly important in double-barrier structures with either vary narrow wells or barrier layers is phonon-assisted tunneling due to symmetric interface modes.[5] We have recently performed calculations[30] which indicate the importance of phonon-assisted tunneling due to symmetric interface modes (which have AlAs phonon energies, i.e., 50.1 meV, and are associated with the two inner heterointerfaces) in structures with narrow well layers (<100 Å). At the same time, structures with very narrow barrier layers (<25 Å) show strong effects due to other symmetric interface modes which are associated with the outer heterointerfaces and have GaAs phonon energies, i.e., 36 meV.

Another potentially important effect concerns the influence of the X point in the barrier layers on measured *I-V* curves of DBRT structures. In $Al_xGa_{1-x}As$ layers with $x>0.45$, the X-point minima of the conduction band have lower energy than the Γ-point minimum; thus there is a tendency for electrons to scatter from the Γ point as they tunnel through the $Al_xGa_{1-x}As$ barriers. Experimental and theoretical studies indicate that Γ-to-X conversion becomes significant only for relatively thick barriers (>50 Å) where $x>0.45$;[37-39] thus we may safely neglect this effect in analyzing narrower DBRT structures such as devices A and B from above.

The effects of band nonparabolicity may also become important if the electrons are sufficiently "hot." While there are sophisticated ways of treating such effects, the simplest method is to define an energy-dependent effective mass. This has been found to give good agreement between theory and experiment[22] and we note that such an energy-dependent effective mass can be easily incorporated into our transfer-matrix calculation. Finally, we note that other complex effects such as many-electron interactions,[40] interface scattering,[41] impurity, and trap state scattering[42-44] can be important in certain real devices. The possible role of such effects in experimental measurements depends sensitively on device parameters and should be considered in constructing a complete picture of resonant tunneling in double barrier structures.

ACKNOWLEDGMENTS

We would like to thank Michael A. Stroscio, Theda Daniels-Race, and Berndt Müller for helpful conversations.

[1]W. R. Frensley, Rev. Mod. Phys. **62**, 745 (1990).
[2]W. R. Frensley, J. Vac. Sci. Technol. B **3**, 1261 (1985).
[3]M. C. Payne, J. Phys. C **19**, 1145 (1986).
[4]R. Tsu and L. Esaki, Appl. Phys. Lett. **22**, 562 (1973).
[5]N. Mori and T. Ando, Phys. Rev. B **40**, 6175 (1989).
[6]B. K. Ridley, Phys. Rev. B **39**, 5282 (1989).
[7]N. S. Wingreen, K. W. Jacobsen, and J. W. Wilkins, Phys. Rev. Lett. **61**, 1396 (1988).
[8]M. Jonson, Phys. Rev. B **39**, 5924 (1989).
[9]W. Cai, T. F. Zheng, P. Hu, B. Yudanin, and M. Lax, Phys. Rev. Lett. **63**, 418 (1989).
[10]V. J. Goldman, D. C. Tsui, and J. E. Cunningham, Phys. Rev. B **36**, 7635 (1987).
[11]M. L. Leadbeater, E. S. Alves, L. Eaves, M. Henini, O. H. Hughes, A. Celeste, J. C. Portal, G. Hill, and M. A. Pate, Phys. Rev. B **39**, 3438 (1989).
[12]F. Chevoir and B. Vinter, Appl. Phys. Lett. **55**, 1859 (1989).
[13]M. V. Klein, IEEE J. Quantum Electron. **QE-22**, 1760 (1986).
[14]R. Fuchs and K. L. Kliewer, Phys. Rev. **140**, A2076 (1965).
[15]M. A. Stroscio, Phys. Rev. B **40**, 6428 (1989).
[16]J. Menéndez, J. Lumin. **44**, 285 (1989).
[17]M. Babiker, J. Phys. C **19**, 683 (1986).
[18]Y. Ando and T. Itoh, J. Appl. Phys. **61**, 1497 (1987).
[19]P. J. Turley, S. W. Teitsworth, and P. Bhattacharya (unpublished).
[20]E. Gerjuoy and D. D. Coon, Superlatt. Microstruct. **5**, 305 (1989).
[21]H. C. Casey and M. B. Panish, *Heterostructure Lasers* (Academic, New York, 1978), Pt. A, Chap. 4.
[22]P. England, J. R. Hayes, M. Helm, J. P. Harbison, L. T. Flores, and S. J. Allen, Appl. Phys. Lett. **54**, 1469 (1989).
[23]D. D. Coon and H. C. Liu, Appl. Phys. Lett. **47**, 172 (1985).
[24]B. Ricco and M. Ya. Azbel, Phys. Rev. B **29**, 1970 (1984).
[25]E. H. Hauge and J. A. Støvneng, Rev. Mod. Phys. **61**, 917 (1989).
[26]J. R. Barker, Physica B **134**, 22 (1985).
[27]S. Collins, D. Lowe, and J. R. Barker, J. Phys. C **20**, 6213 (1987).
[28]A. P. Jauho and M. M. Nieto, Superlatt. Microstruct. **2**, 407 (1986).
[29]A. Messiah, Quantum Mechanics (Wiley, New York, 1958), Vol. 1.
[30]P. J. Turley and S. W. Teitsworth (unpublished).
[31]U. Sivan, M. Heiblum, and C. P. Umbach, Phys. Rev. Lett. **63**, 992 (1989).
[32]T. W. Hickmott, P. M. Solomon, F. F. Fang, F. Stern, R. Fischer, and H. Morkoç, Phys Rev Lett. **52**, 2053 (1984).
[33]The matrix elements for the right-hand barrier are not shown

because the nonresonant wave functions are very small there, as can be seen in Fig. 5. As a result, the contribution of confined phonon modes in the right-hand barrier to the phonon-assisted tunneling signal will be exceedingly small.

[34]J. A. Kash, S. S. Jha, and J. C. Tsang, Phys. Rev. Lett. **58**, 1869 (1987).

[35]D. W. Nam, N. Holonyak, E. J. Vesely, and R. D. Dupuis, Appl. Phys. Lett. **57**, 46 (1990).

[36]W. R. Frensley, in *Nanostructure Physics and Fabrication,* edited by M. A. Reed and W. P. Kirk (Academic, New York, 1989), p. 231.

[37]D. Landheer, H. C. Liu, M. Buchanan, and R. Stoner, Appl. Phys. Lett. **54**, 1784 (1989).

[38]E. E. Mendez, W. I. Wang, E. Calleja, and C. E. T. Gonçalves da Silva, Appl. Phys. Lett. **50**, 1263 (1987).

[39]H. C. Liu, Superlatt. Microstruct. **7**, 35 (1990).

[40]T. K. Ng and P. A. Lee, Phys. Rev. Lett. **61**, 1768 (1988).

[41]D. D. Coon and H. C. Liu, Superlatt. Microstruct. **6**, 409 (1989).

[42]A. D. Stone and P. A. Lee, Phys. Rev. Lett. **50**, 1503 (1987).

[43]M. Büttiker, IBM, J. Res. Dev. **32**, 63 (1988).

[44]H. A. Fertig and S. Das Sarma, Phys. Rev. B **40**, 7410 (1989).